

## *Supporting Information*

# **Application and Limitations of Nanocasting in Metal-Organic Frameworks**

Camille D. Malonzo,<sup>1,†</sup> Zhao Wang,<sup>1,†</sup> Jiaxin Duan,<sup>1</sup> Wenyang Zhao,<sup>1</sup> Thomas E. Webber,<sup>1</sup> Zhanyong Li,<sup>2</sup> In Soo Kim,<sup>3,4</sup> Anurag Kumar,<sup>5</sup> Aditya Bhan,<sup>5</sup> Ana E. Platero-Prats,<sup>6,7</sup> Karena W. Chapman,<sup>6</sup> Omar K. Farha,<sup>2,8</sup> Joseph T. Hupp,<sup>2</sup> Alex B. F. Martinson,<sup>3</sup> R. Lee Penn,<sup>1</sup> Andreas Stein<sup>1,\*</sup>

<sup>1</sup>*Department of Chemistry, University of Minnesota, Minneapolis, Minnesota 55455, United States*

<sup>2</sup>*Department of Chemistry, Northwestern University, Evanston, Illinois 60208, United States*

<sup>3</sup>*Materials Science Division, Argonne National Laboratory, Argonne, Illinois 60439, United States*

<sup>4</sup>*Current address: Nanophotonics Research Center, Korea Institute of Science and Technology, Seoul 02792, South Korea*

<sup>5</sup>*Department of Chemical Engineering and Materials Science, University of Minnesota, Minneapolis, Minnesota 55455, United States*

<sup>6</sup>*X-ray Science Division, Advanced Photon Source, Argonne National Laboratory, Argonne, Illinois 60439, United States*

<sup>7</sup>*Current address: Department of Inorganic Chemistry, Universidad Autónoma de Madrid, 28049 Madrid, Spain*

<sup>8</sup>*Department of Chemistry, Faculty of Science, King Abdulaziz University, Jeddah, Saudi Arabia*

<sup>†</sup>These authors contributed equally.

\*Corresponding author: a-stein@umn.edu

## Experimental Methods

### Materials

The following chemicals were used as received:  $\text{ZrOCl}_2 \cdot 8\text{H}_2\text{O}$  (98%),  $(\text{NH}_4)_2\text{Ce}(\text{NO}_3)_6$  ( $\geq 98.5\%$ ),  $\text{Ni}(\text{NO}_3)_2 \cdot 6\text{H}_2\text{O}$  ( $\geq 97\%$ ), benzene-1,4-dicarboxylic acid ( $\text{H}_2\text{bdc}$ , 98%), benzene-1,3,5-tribenzoic acid ( $\text{H}_3\text{btb}$ ,  $\geq 98\%$ ), benzene-1,3,5-tricarboxylic acid (trimesic acid,  $\text{H}_3\text{btc}$ , 95%), tetramethyl orthosilicate (TMOS, 98%), and methanol ( $\geq 99.8\%$ ) from Sigma-Aldrich, biphenyl-4,4'-dicarboxylic acid ( $\text{H}_2\text{bpdc}$ , ( $\geq 97.0\%$ ) from TCI America, hydrochloric acid (36.5–38.0%) and formic acid (88–91%) from BDH Chemicals, *N,N*-dimethylformamide (DMF, 99.8%) from Macron Fine Chemicals, *N,N*-diethylformamide (DEF, 99%) from Acros Organics, dimethylsulfoxide (DMSO, 99.9%) from Fisher Chemical, and ethanol (100%) from Pharmco-Aaper. Deionized water produced on-site with a minimum resistivity of 18.2  $\text{M}\Omega \cdot \text{cm}$  was used in all experiments.

### Synthesis of MOFs

*UiO-66*. The procedure for the preparation of (Zr)UiO-66 was similar to the one described in the literature.<sup>1</sup>  $\text{ZrOCl}_2 \cdot 8\text{H}_2\text{O}$  (125 mg, 0.54 mmol) was dissolved in a mixture of DMF (5 mL) and concentrated HCl (1 mL). In a separate vial, the linker,  $\text{H}_2\text{bdc}$  (123 mg, 0.75 mmol) was also dissolved in DMF (10 mL). The two solutions were mixed and heated at 80 °C for 24 h. The product, (Zr)UiO-66, was washed twice with DMF and then twice with methanol prior to air-drying. The MOF was finally activated at 150 °C for 12 h.

*(Ce)UiO-66 and (Ce)UiO-67*. The procedure for the preparation of (Ce)UiO-66 and (Ce)UiO-67 was adapted from a previous publication.<sup>2</sup> To synthesize (Ce)UiO-66,  $\text{H}_2\text{bdc}$  (35.4 mg, 0.213 mmol) was dissolved in DMF (1.2 mL). In a separate vial,  $(\text{NH}_4)_2\text{Ce}(\text{NO}_3)_6$  (117 mg, 0.21 mmol) was dissolved in deionized water (0.4 mL). The two solutions were mixed and heated at 100 °C for 15 min. The product, (Ce)UiO-66, was washed twice with DMF and then twice with methanol prior to air-drying. The MOF was finally activated at 130 °C for 12 h. (Ce)UiO-67 was prepared similarly, with the following exceptions:  $\text{H}_2\text{bpdc}$  (51.6 mg, 0.213 mmol) was used as the linker, the reaction time at 100 °C was increased from 15 min to 20 min, and the sample was washed twice with DMSO instead of DMF.

*(Ce)MOF-808*. The procedure for the preparation of (Ce)MOF-808 was adapted from a previous publication.<sup>3</sup> To synthesize (Ce)MOF-808, H<sub>3</sub>btc (22.4 mg, 0.106 mmol) was introduced into a vial containing a mixture of DMF (1.2 mL) and formic acid (0.578 mL, 6.83 mmol). A solution of (NH<sub>4</sub>)<sub>2</sub>Ce(NO<sub>3</sub>)<sub>6</sub> (0.6 mL, 0.533 M) was then added to this mixture. The vial was heated at 100 °C for 15 min. The product, (Ce)MOF-808, was washed twice with DMF and then four times with acetone prior to 70 °C air-drying. The MOF was finally activated at 100 °C for 12 h.

*DUT-9*. The procedure for the preparation of DUT-9 was adapted from the literature.<sup>4</sup> H<sub>3</sub>btb (90 mg, 0.20 mmol) and Ni(NO<sub>3</sub>)<sub>2</sub>·6H<sub>2</sub>O (183 mg, 0.63 mmol) were dissolved in DEF (5.25 mL) in a vial. The solution was heated at 120 °C for 20 h. The product, DUT-9, was washed twice with DMF, which was then exchanged with 100% ethanol prior to supercritical CO<sub>2</sub> (sc-CO<sub>2</sub>) drying.

Supercritical drying was performed on a Tousimis Samdri-780A critical point dryer. The sample was placed in fresh 100% ethanol immediately before placing it inside the dryer. The sample was purged with liquid CO<sub>2</sub> at 0–10 °C for 6 min and then soaked in it for 2 h. The CO<sub>2</sub> was then brought above the supercritical point (at 1100–1300 psi and 33–41 °C) and released from the dryer. The sc-CO<sub>2</sub>-dried DUT\_9 was heated to 60 °C for 12 h to complete the activation.

### **Preparation of Metal-Modified MOFs**

*Ni(SIM)-NU-1000*. Nickel(II) acetate tetrahydrate (276.5 mg, 1.11 mmol) was suspended in 40 mL DMF in a 100-mL screw cap jar. It was subsequently incubated in an oven at 100 °C for 30 min or until the solution became clear. Next, NU-1000 (400 mg, 0.185 mmol) was added to the jar, and it was subjected to 5 min of sonication before being incubated in an oven at 100 °C overnight. The suspension was centrifuged, and the mother liquor was decanted while hot after centrifugation. The solid residue was washed with hot DMF three times (3 × 50 mL) or until the DMF solution was colorless. The recovered solid material was immersed in acetone for one hour and then washed three times (30 min intervals) to remove the residual DMF by solvent exchange. After subsequent suspension in acetone for another 8 h, the yellow solid material was placed in a vacuum oven (< 100 mTorr, room temperature) for 2 h before it was thermally activated at

120 °C on a Smart VacPrep instrument for 24 h. The recovered material, denoted as Ni(SIM)-NU-1000, was kept in a vacuum desiccator for storage.

*In(AIM)-NU-1000.* Indium-loaded NU-1000 was synthesized via ALD in MOFs (AIM) using a modified procedure described previously.<sup>5</sup> In each experiment, 50 mg of NU-1000 powder was heated to 125 °C under suction with a continuous flow of 20 sccm nitrogen (N<sub>2</sub>), resulting in 0.4 Torr – standard “purge” conditions. After 10 min of purge conditions to remove any physisorbed water, the powder was reproducibly hydroxylated with a 60 s exposure to water vapor using a pulse sequence of t<sub>1</sub>-t<sub>2</sub>-t<sub>3</sub> (pulse length – exposure – purge), where t<sub>1</sub> = 1 s, t<sub>2</sub> = 59 s, t<sub>3</sub> = 300 s. Subsequently, the powder was purged for 5 min to remove physisorbed water and obtain a steady –OH and –OH<sub>2</sub> population. Trimethylindium (InMe<sub>3</sub>) was then introduced into the reaction chamber using the same pulse sequence, but with standard pulse times of t<sub>1</sub> = 0.1 s, t<sub>2</sub> = 29.9 s, and t<sub>3</sub> = 30 s. Following 800 repeated exposures of InMe<sub>3</sub>, the sample was left to purge for an additional 5 min to ensure a complete removal of any excess precursor and/or reaction by-products within the pores of NU-1000. The powder was then subjected to 80 doses of water vapor according to the previous dosing schedule, but with a shorter pulse length (0.1 s) in order to minimize the effects of MOF heating expected from the strongly exothermic heat of reaction.

### **Silica Nanocasting**

*Silica Nanocasting with Acid Catalyst.* A casting solution composed of 300 μL of TMOS, 5 μL of methanol and 5 μL H<sub>2</sub>O was first mixed in a vial. It was then added to 30 mg of the MOF and allowed to infiltrate the MOF particles for 24 h. Afterwards, the sample was washed with methanol to remove any TMOS from the external surface of the particles, and heated at 40 °C for 5 min to dry. To induce hydrolysis and condensation of the TMOS in the sample, the sample was first exposed to HCl(g) for 24 h at room temperature. This was followed by heat treatment in a closed vial at 60 °C for another 24 h. Finally, the sample was calcined at 500 °C for 1 h in static air to remove the organic linkers from the structure. A temperature ramp rate of 2 °C min<sup>-1</sup> was used for calcination.

*Silica Nanocasting without Acid Catalyst.* A casting solution composed of 300 μL of TMOS, 75 μL of methanol and 50 μL H<sub>2</sub>O was first mixed in a vial. It was then added to 30 mg of the MOF and allowed to infiltrate the MOF particles for 24 h. The casting solution was removed by centrifugation and decantation. Afterwards, the sample was washed with methanol to remove any

TMOS from the external surface of the particles, and heated at 40 °C for 5 min to dry. To induce hydrolysis and condensation of the TMOS in the sample, the sample was heated in a closed vial at 80 °C for 24 h. Finally, the sample was calcined at 500 °C for 1 h to remove the organic linkers from the structure. A temperature ramp rate of 2 °C min<sup>-1</sup> was used for calcination.

A modified procedure for nanocasting DUT-9 was carried out as follows. After the synthesized MOF was washed twice with DMF, the DMF was replaced with the casting solution composed of 300 µL of TMOS, 75 µL of methanol and 50 µL H<sub>2</sub>O. The exchange was allowed to proceed for 3 days. The casting solution was removed by centrifugation and decantation, and the MOF particles were treated as described above to yield the final nanocast material.

The maximum theoretical loading of silica inside the pores of the MOFs was estimated assuming that all pore space in the MOFs is occupied by the TMOS precursor and transformed into amorphous silica. If the pore volume of the host MOF is  $V_{MOF}$ , then the volume fraction occupied by silica after condensation ( $V_{silica}$ ) is:

$$V_{silica} = \frac{d_{TMOS} \times V_{MOF}}{M_{TMOS}} \times \frac{M_{amorphous\ silica}}{d_{amorphous\ silica}}$$

Here,  $d_{TMOS} = 1.03 \text{ g/cm}^3$  and  $d_{amorphous\ silica} = 2.20 \text{ g/cm}^3$  are the densities of TMOS and amorphous silica, respectively, and  $M_{TMOS} = 152.22 \text{ g/mol}$  and  $M_{amorphous\ silica} = 60.08 \text{ g/mol}$  the corresponding molar masses. Using this equation, the maximum volume fraction of silica obtained from TMOS after condensation is always 0.185 (or 18.5%) that of the available pore volume.

## Characterization

FT-IR spectra were collected on a Nicolet Magna-IR 760 spectrometer. Ground samples were placed between two KBr windows for FT-IR measurements. Scanning electron microscopy (SEM) measurements were performed on a JEOL 6700 scanning electron microscope operated using a 5.0 kV accelerating voltage. Prior to SEM analysis, all samples were sputter coated with a conductive thin film (70 Å) of Pt. X-ray diffraction (XRD) patterns were collected using an X'Pert Pro diffractometer with an X'Celerator detector. A Co anode (K $\alpha$ ,  $\lambda = 1.789 \text{ \AA}$ ) operated at 45 kV and 40 µA was used as the radiation source. N<sub>2</sub> sorption analyses were conducted using

a Quantachrome Autosorb iQ2. The MOF samples were degassed prior to the analysis at 1 mTorr for 12 h at the following temperatures: (Zr)UiO-66, (Ce)UiO-66, and (Ce)UiO-67 at 130 °C, DUT-9 at 60 °C, and Ni(SIM)-NU-1000 and In(AIM)-NU-1000 at 120 °C. Scanning electron microscopy-energy-dispersive X-ray spectroscopy (EDS) compositional analyses were acquired on a JEOL JXA-8900 electron microprobe operated at 15.0 kV accelerating potential. Samples were coated with a thin film (70 Å) of carbon prior to SEM-EDS measurements.

Scanning transmission electron microscopy–energy dispersive X-ray spectroscopy (STEM-EDS) was performed using an FEI Tecnai G2 field-emission S/TEM operating at an accelerating voltage of 80 kV. The nanocast samples were loaded onto TEM grids from ethanol suspensions. High-angle annular dark field (HAADF) images were collected on an E. A. Fischione annular detector using an inner collection semiangle of 21.7 mrad. EDS spectra were obtained using a ChemiSTEM EDX spectrometer. EDS maps were collected while rastering the beam over the sample, which facilitated minimization of beam damage. A probe current of ~0.1 nA was used, and maps were collected over a minimum of 5 min. Data were analyzed using ESPRIT software (version 1.9.4). X-ray photoelectron spectroscopy (XPS) was performed using a VersaProbe III instrument, with a Al K- $\alpha$  X-ray source.

Powder X-ray diffraction (XRD) data and total scattering data suitable for pair distribution function (PDF) analysis were collected at beamlines 17-BM and 11-ID-B, respectively, at the Advanced Photon Source at Argonne National Laboratory using 27.4 keV (0.45220 Å) and 58.6 keV (0.2114 Å) X-rays, respectively. Data were collected using amorphous silicon-based area detectors. Geometric corrections and reduction to one-dimensional data used GSAS-II<sup>6</sup> and FIT2D.<sup>7</sup>

PDFs were obtained from the data within PDFgetX3<sup>8</sup> to a  $Q_{\max}=24 \text{ \AA}^{-1}$ . Differential PDFs were calculated by subtracting the PDF measured for SiO<sub>2</sub> from the calcined nanocast samples within Fityk.<sup>9</sup> PDFs for structural models were simulated in PDFgui.<sup>10</sup>

### **Catalyst Testing: Cyclohexane Dehydrogenation**

Nanocast NU-1000 was prepared by silica nanocasting using the acid catalyst procedure described above. The nanocast material (0.015 g, mesh 40-80) was heated from room temperature to 610 °C under a flow of air (100 mL min<sup>-1</sup>) for an hour and kept at temperature for another hour. The temperature was measured using a thermocouple probe in the middle of the

catalyst bed. At this temperature, the reaction mixture consisting of a 1:8.31 molar ratio of cyclohexane and H<sub>2</sub> (0.95 kPa cyclohexane/7.90 kPa H<sub>2</sub>/balance Ar and CH<sub>4</sub>) was fed to the catalyst bed at a flow rate of 42 cm<sup>3</sup> min<sup>-1</sup>. The results are shown in Figure S1.

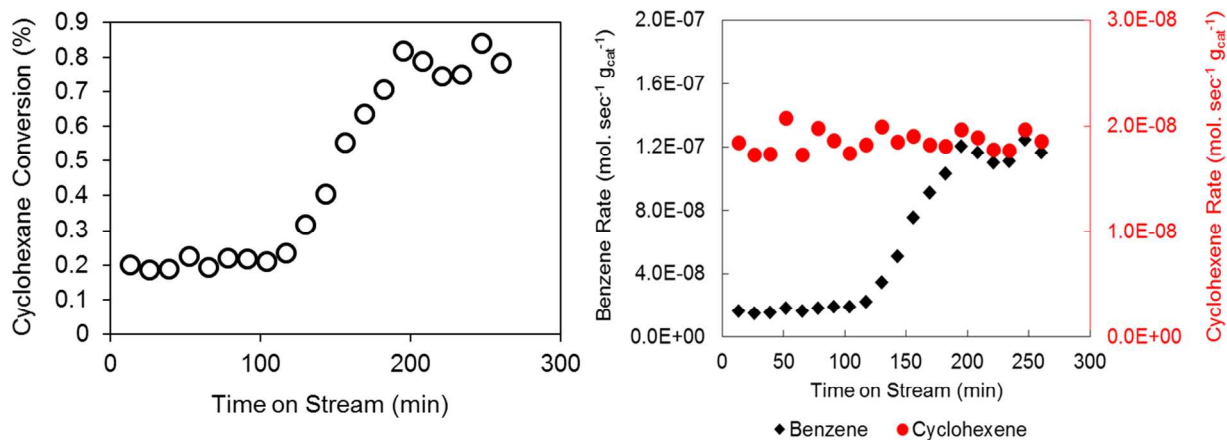


**Figure S1.** Catalytic activity of nanocast NU-1000 in cyclohexane dehydrogenation. Cyclohexane conversion is below 1%. The products are cyclohexene and benzene, with an induction period observed for benzene production.

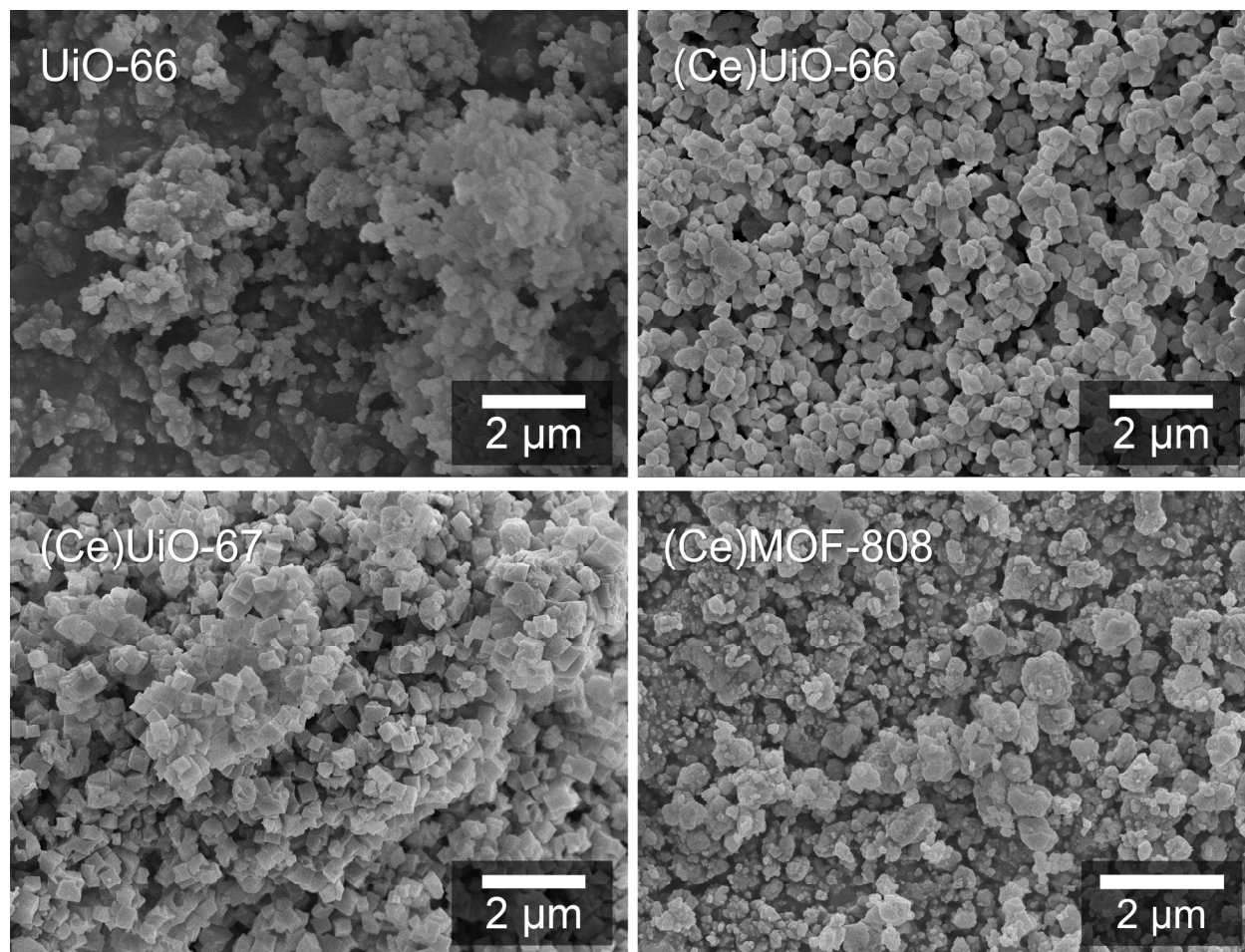


**Figure S2.** SEM images of the synthesized UiO-66 and (Ce)MOFs.

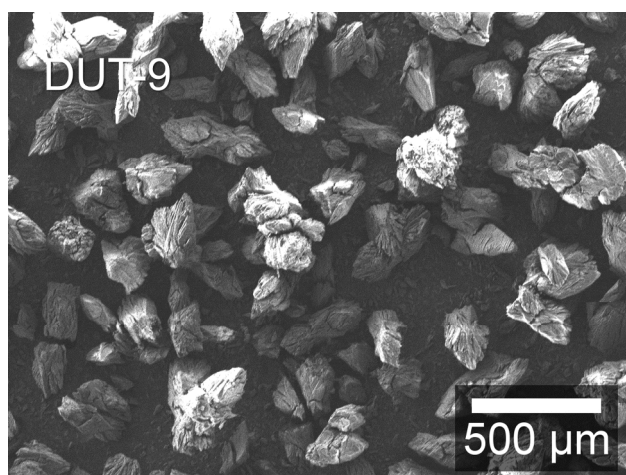


**Figure S3.** SEM image of DUT-9.

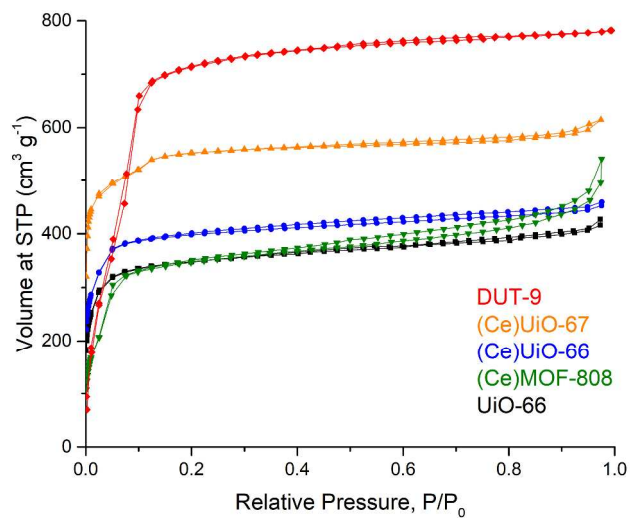


**Figure S4.** N<sub>2</sub> sorption isotherms of the synthesized MOFs.

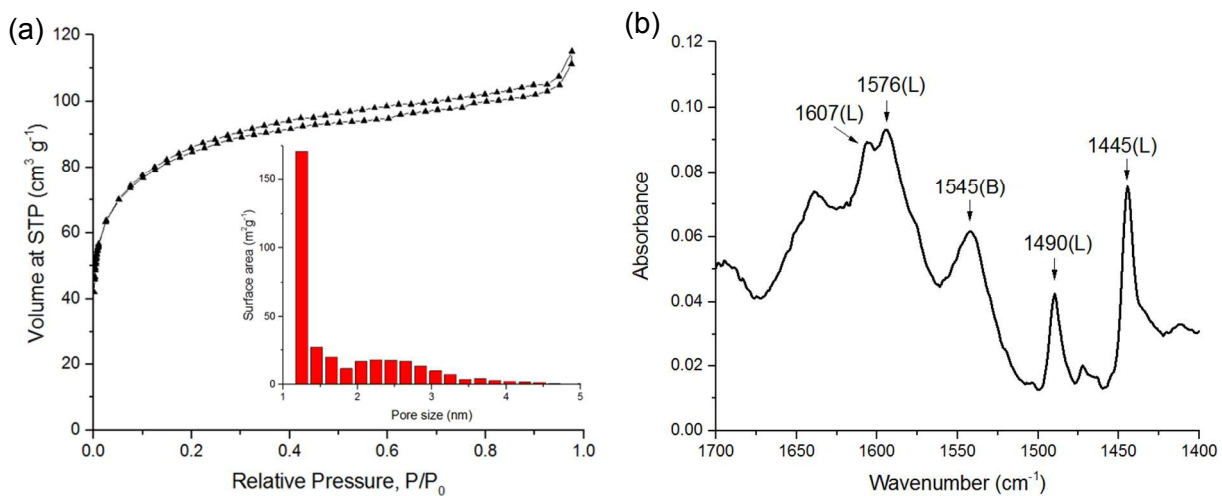


**Figure S5.** (a) N<sub>2</sub> sorption isotherm and surface area histogram (inset) of nanocast UiO-66 showing micro- and mesoporosity in the material, and (b) IR spectrum after pyridine adsorption on nanocast UiO-66. The peaks labeled L and B denote pyridine adsorbed on Lewis and Brønsted acid sites, respectively.

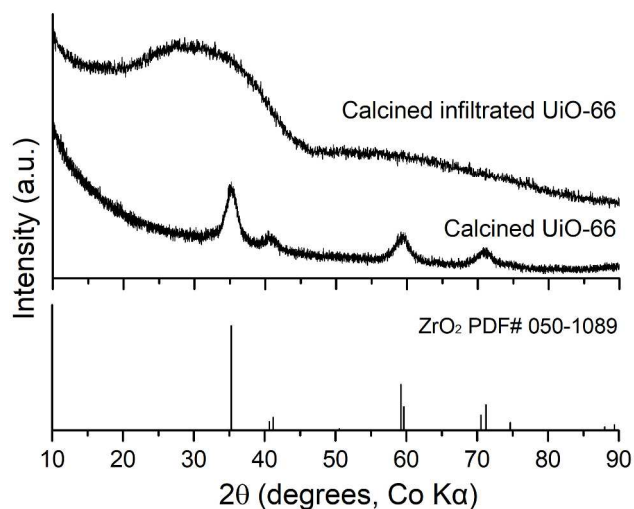


**Figure S6.** XRD patterns of calcined UiO-66 (500 °C, 1 h) and calcined, TMOS-infiltrated UiO-66 samples.

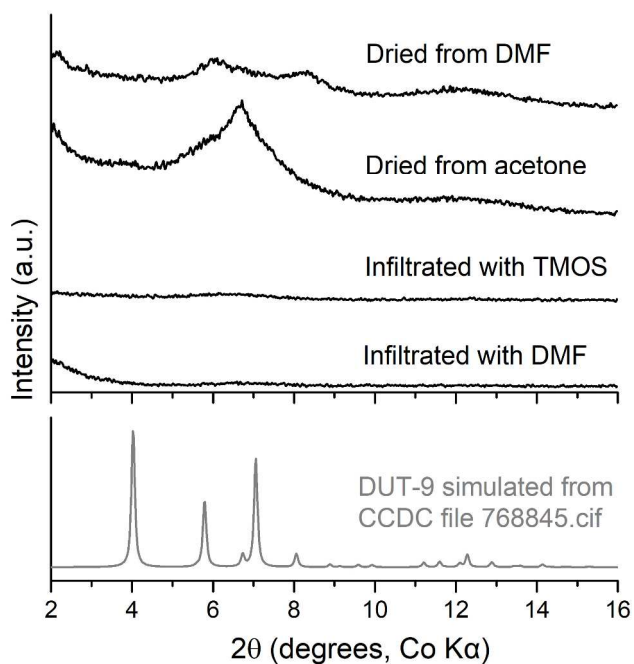


**Figure S7.** XRD patterns of DUT-9 showing effects of capillary forces on the MOF. Air-drying DUT-9 from DMF results in structural collapse indicated by the loss of the characteristic XRD pattern of the MOF. Conventional drying by exchanging the DMF with acetone followed by air-drying also results in a collapsed framework. Infiltration of an activated DUT-9 sample with TMOS or DMF yields the same result. The XRD patterns of the infiltrated samples were taken after 24 h of infiltration, and the samples were wetted with the corresponding solvent during XRD data collection.

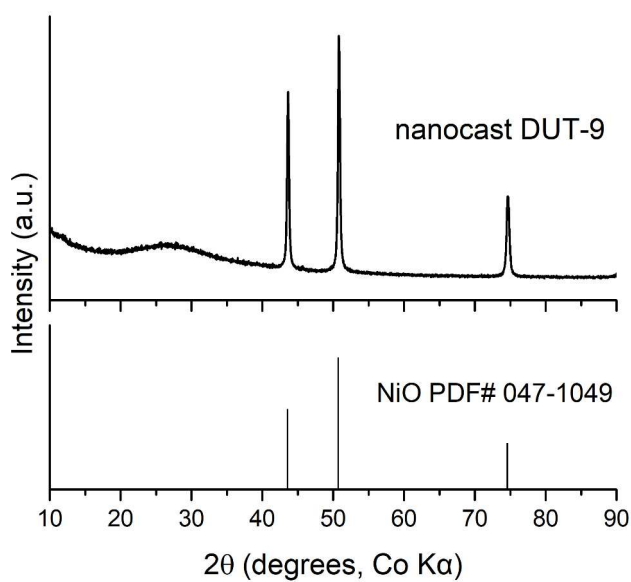


**Figure S8.** XRD pattern of nanocast DUT-9 prepared by a modified procedure where the casting fluid is introduced into the MOF pores by solvent exchange instead of infiltration of an activated sample. The rest of the procedure is the same as that outlined for silica nanocasting with an acid catalyst.

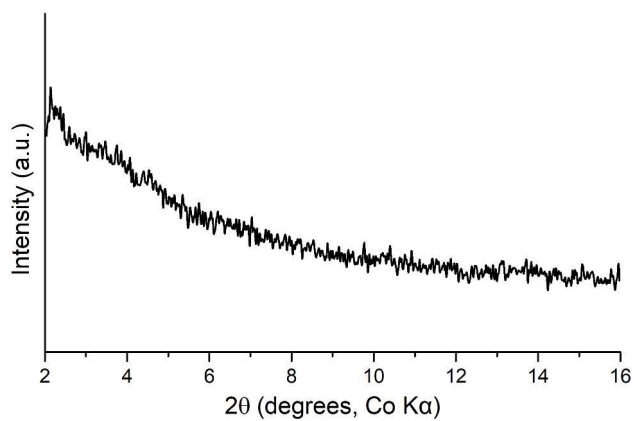


**Figure S9.** XRD pattern of DUT-9 after exposure to HCl(g) for 24 h.

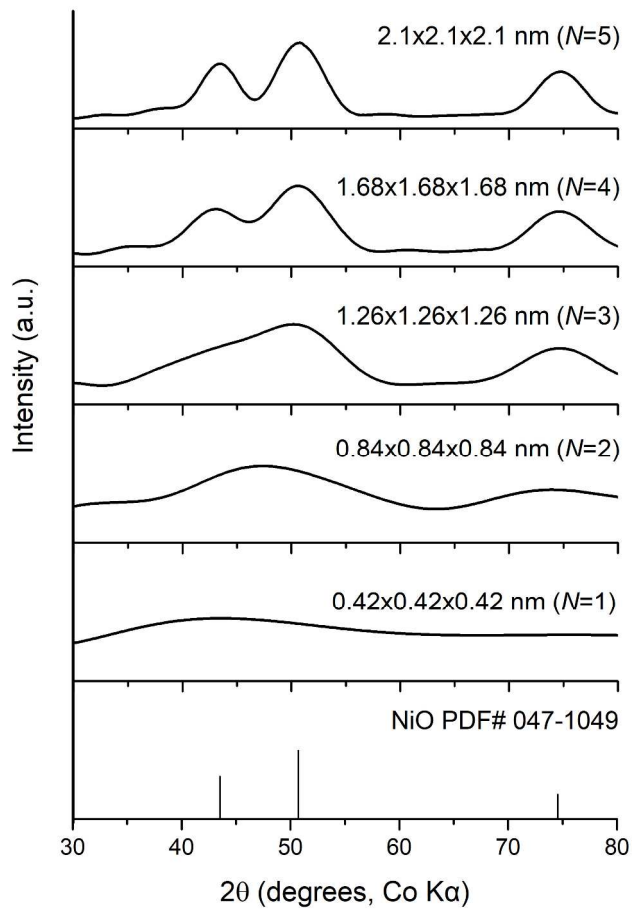


**Figure S10.** Standard stick pattern and XRD diffraction patterns of cubic NiO (PDF# 47-1049) with various crystallite sizes, simulated using *SKIP* software.<sup>11</sup>  $N$  corresponds to the number of unit cells along each  $a$ ,  $b$ , and  $c$  direction with crystallite sizes labeled.

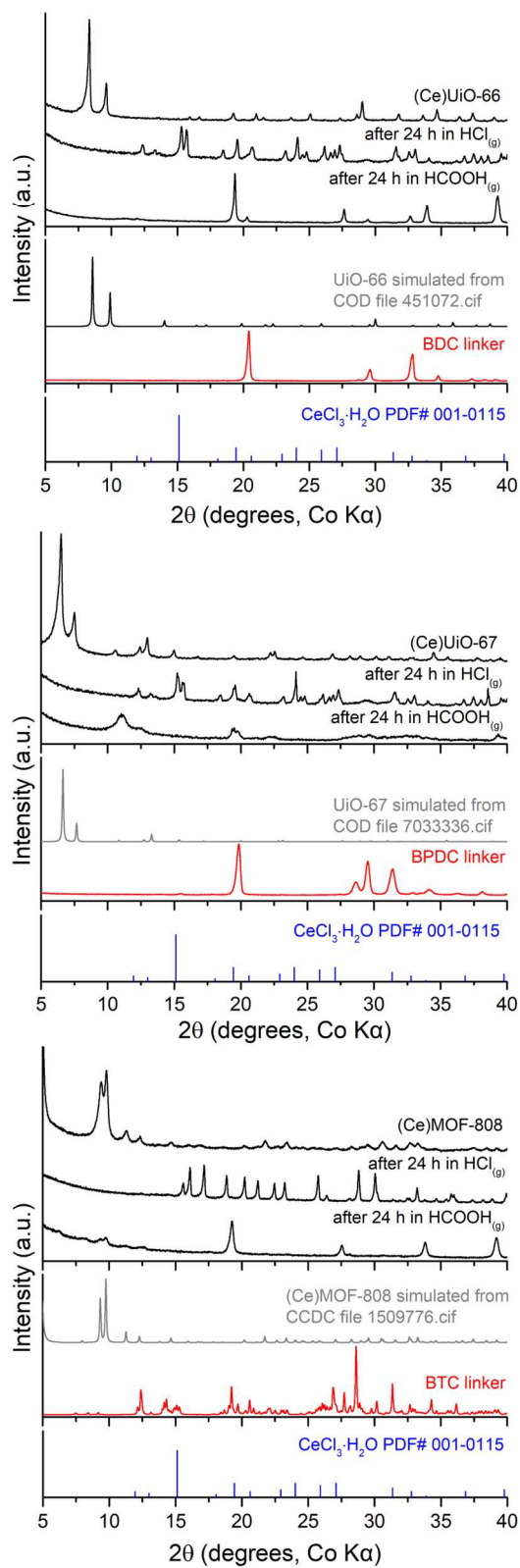


**Figure S11.** XRD patterns of (Ce)UiO-66, (Ce)UiO-67, and (Ce)MOF-808 after exposure to  $\text{HCl}_{(g)}$  and  $\text{HCOOH}_{(g)}$  for 24 h. The pattern for the MOFs after exposure to  $\text{HCl}_{(g)}$  corresponds to hydrated  $\text{CeCl}_3$ .

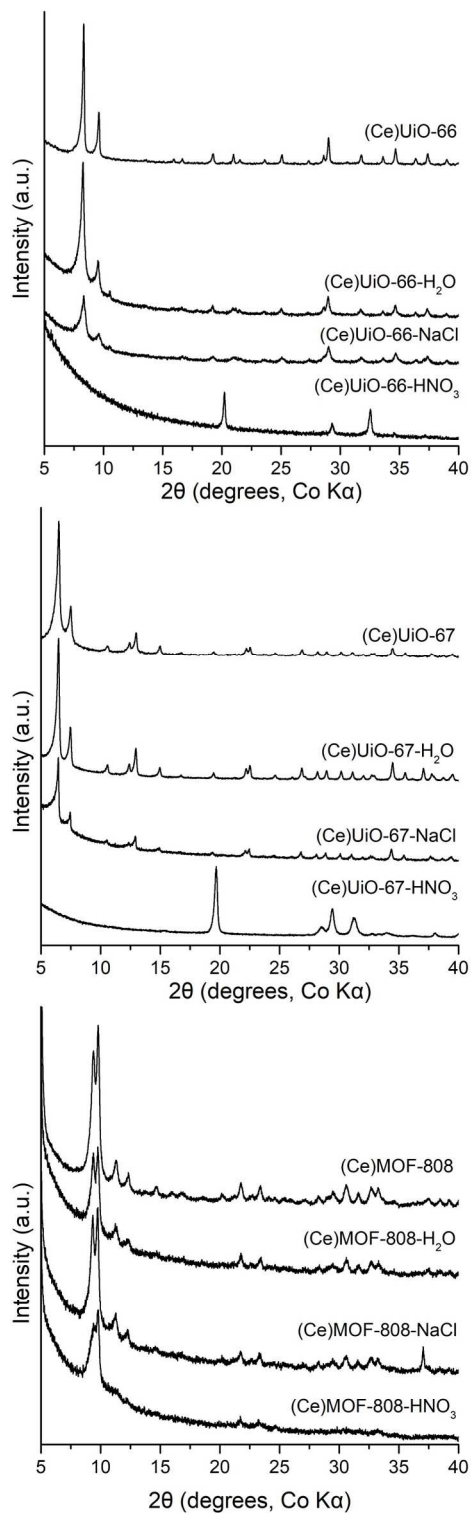


**Figure S12.** XRD patterns of (Ce)UiO-66, (Ce)UiO-67, and (Ce)MOF-808 samples after being soaked in H<sub>2</sub>O, 3 mol/L NaCl solution or 3 mol/L HNO<sub>3</sub> solution for 24 h. The samples were then washed with acetone and dried at 70 °C for 10 min.

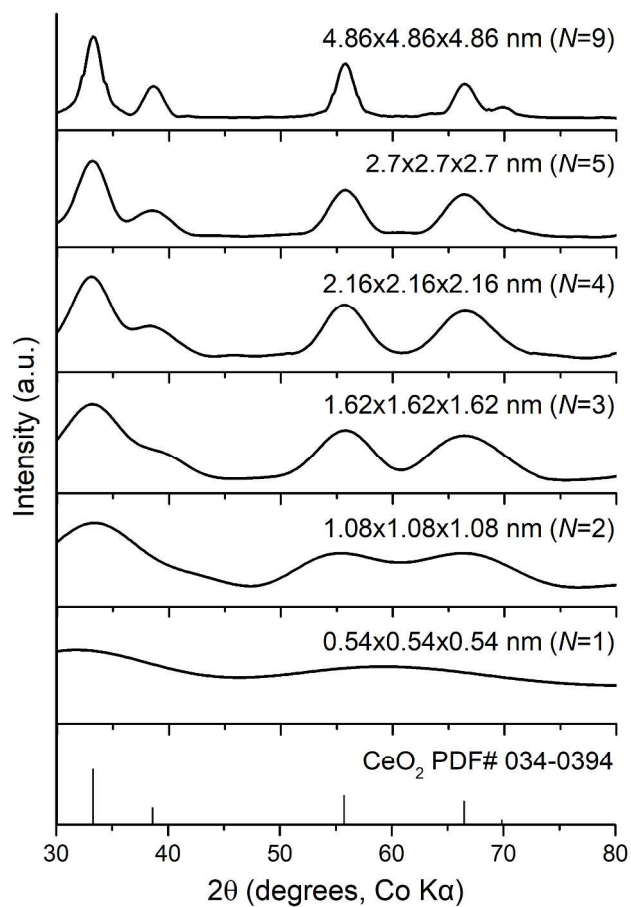


**Figure S13.** Standard stick pattern and XRD diffraction patterns of cubic  $\text{CeO}_2$  (PDF# 34-0394) with various crystallite sizes, simulated using *SKIP* software.<sup>11</sup>  $N$  corresponds to the number of unit cells along each  $a$ ,  $b$ , and  $c$  direction with crystallite sizes labeled.

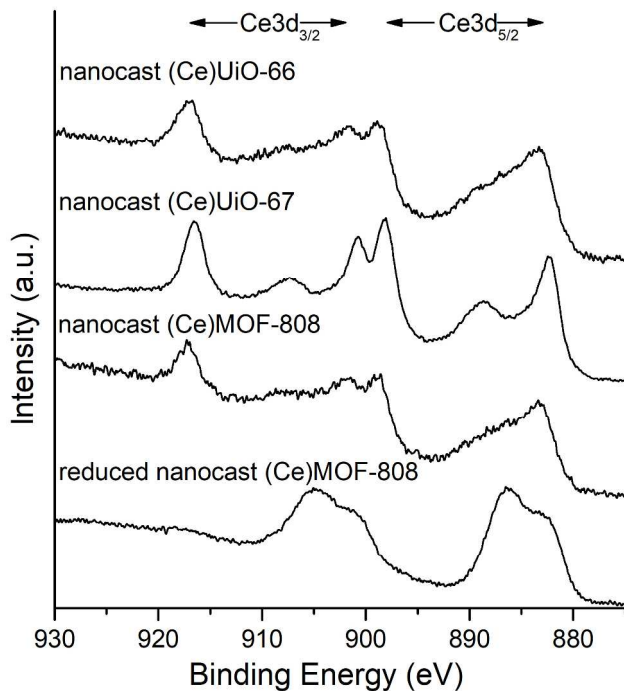


**Figure S14.** XPS spectra of nanocast (Ce)UiO-66, nanocast (Ce)UiO-67, nanocast (Ce)MOF-808, and reduced nanocast (Ce)MOF-808 samples. Reduction of nanocast (Ce)MOF-808 was performed at 750 °C for 1 h in a mixture of 95% N<sub>2</sub> and 5% H<sub>2</sub> with a flow rate of 600 mL/min. The peak at around 917 eV for the three nanocast samples is characteristic for the presence of Ce<sup>4+</sup>, which was further confirmed by the disappearance of this peak in the reduced nanocast (Ce)MOF-808 sample. The peak at around 886 eV in the reduced sample can be assigned to Ce<sup>3+</sup>, but it is not pronounced in the three nanocast samples. It is concluded that the majority of Ce species are in the 4+ oxidation state. The Ce<sup>4+</sup>/Ce<sup>3+</sup> ratio could not be determined with certainty because the peaks of Ce<sup>3+</sup> overlap with those of Ce<sup>4+</sup>.

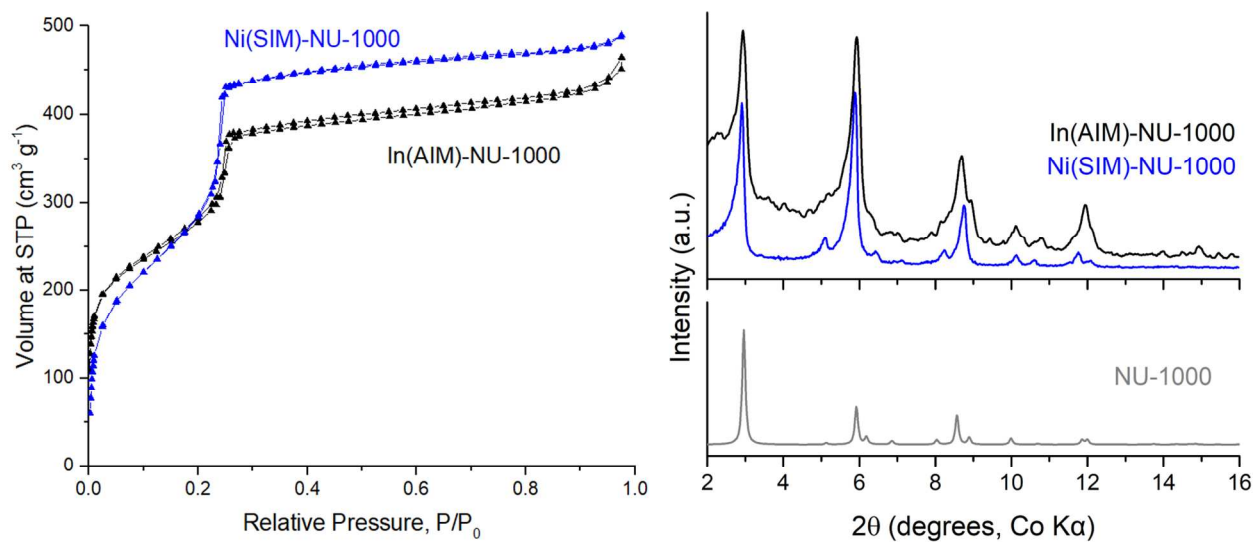


**Figure S15.** N<sub>2</sub> sorption isotherms (left) and XRD patterns (right) of Ni- and In-loaded NU-1000 (Ni(SIM)-NU-1000 and In(AIM)-NU-1000) prepared by solution deposition and atomic layer deposition, respectively. The BET surface area and pore volume of Ni(SIM)-NU-1000 are 1109 m<sup>2</sup>g<sup>-1</sup> and 0.75 cm<sup>3</sup>g<sup>-1</sup>, respectively. The corresponding values for In(AIM)-NU-1000 are 1028 m<sup>2</sup>g<sup>-1</sup> and 0.70 cm<sup>3</sup>g<sup>-1</sup>. BET surface areas were evaluated based on the guidelines in ref.<sup>12</sup> The BET range for Ni(SIM)-NU-1000 is at  $p/p_0 = 0.05$  to 0.22. The BET range for In(AIM)-NU-1000 is at  $p/p_0 = 0.01$  to 0.25.

## Leaching Test for Ni(SIM)-NU-1000 and In(AIM)-NU-1000

After the infiltrated MOF particles were separated from the casting fluid, the latter was also exposed to HCl(g) for 24 h at room temperature. This was followed by heat treatment in a closed vial at 60 °C for another 24 h. Finally, the sample was calcined at 500 °C for 1 h. A temperature ramp rate of 2 °C min<sup>-1</sup> was used for calcination. The presence of In or Ni in the resulting sample was analyzed by SEM-EDS and XRD. Similar steps were taken for the methanol washings used to remove the TMOS from the external surface of the infiltrated particles.

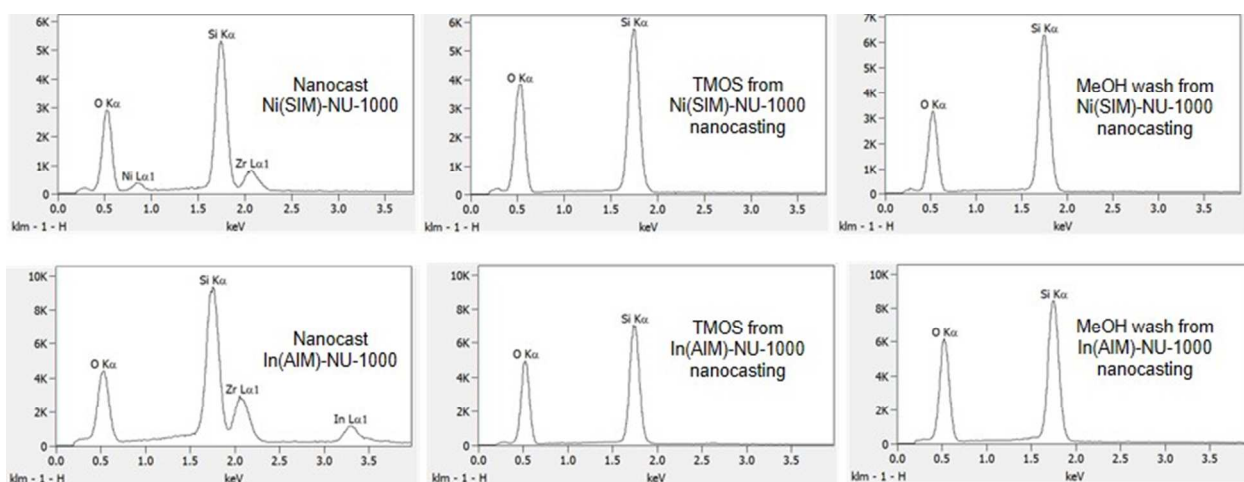


**Figure S16.** SEM-EDS data from the leaching test for Ni(SIM)-NU-1000 (top data) and In(AIM)-NU-1000 (bottom data) nanocasting. The data on the left are for the nanocast samples showing the presence of Ni (~4 Ni per Zr<sub>6</sub>O<sub>8</sub> node) and In (~5 In per Zr<sub>6</sub>O<sub>8</sub> node). No Ni or In was detected in the TMOS casting fluid or the methanol wash for both nanocasting samples.

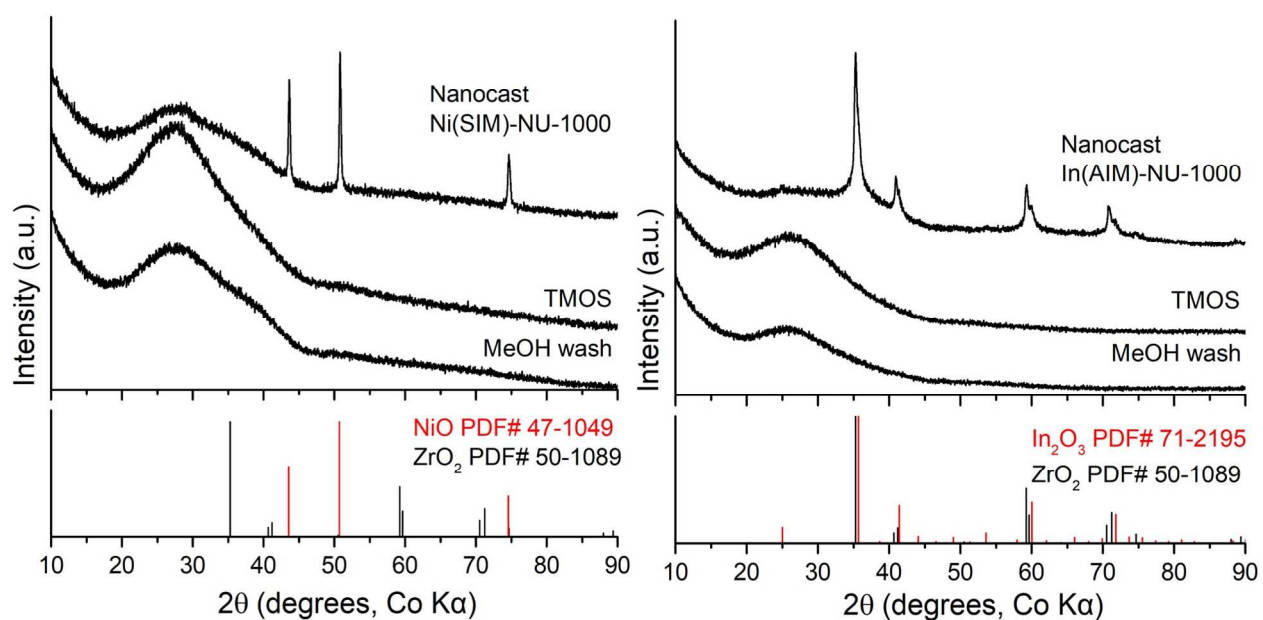


**Figure S17.** XRD patterns obtained after the leaching test for samples prepared by nanocasting in Ni(SiM)-NU-1000 or In(AIM)-NU-1000. No oxides of Ni or In was detected in the TMOS casting fluid or the methanol wash for both nanocasting samples.

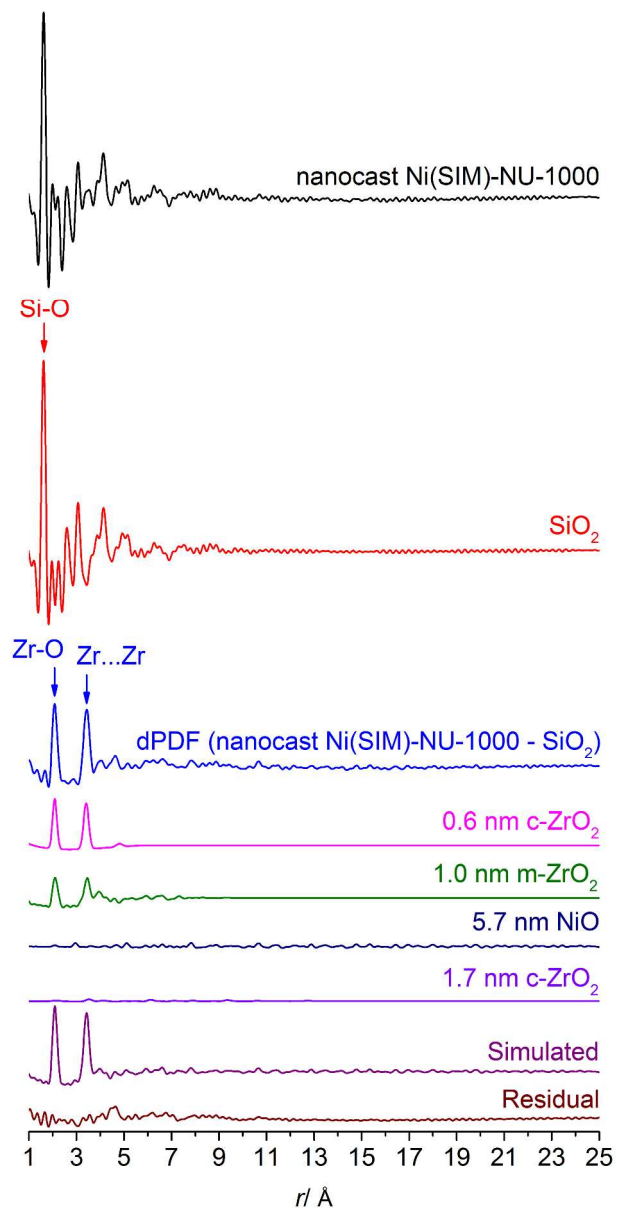


**Figure S18.** PDFs for nanocast Ni(SiM)-NU-1000 and simulated PDF patterns showing Zr-O and Zr...Zr correlations after subtraction of the silica component. The fitting results indicate that the non-silica components in this NiZr<sub>6</sub>@SiO<sub>2</sub> sample mainly consist of single Zr<sub>6</sub> clusters (0.6 nm, cubic,  $a = 4.84 \text{ \AA}$ , ~62 wt%) and distorted monoclinic ZrO<sub>2</sub> (1.0 nm, monoclinic,  $a = 4.97 \text{ \AA}$ ,  $b = 5.31 \text{ \AA}$ ,  $c = 5.14 \text{ \AA}$ ,  $\beta = 100^\circ$ , ~36.4 wt%), both of which would be modified with Ni (not included in the model) to give an average Ni:Zr<sub>6</sub> molar ratio of 3.86. Features beyond 1.0 nm correspond mainly to trace amounts of NiO (5.7 nm, cubic,  $a = 4.18 \text{ \AA}$ , ~1 wt%) and cubic ZrO<sub>2</sub> (1.7 nm, cubic,  $a = 5.00 \text{ \AA}$ , ~0.6 wt%).  $R_w$  is 0.293704. If all Ni had aggregated as NiO, this would amount to ~27 wt%. Note: all of these wt% values exclude silica.

## References

- (1) Katz, M. J.; Brown, Z. J.; Colon, Y. J.; Siu, P. W.; Scheidt, K. A.; Snurr, R. Q.; Hupp, J. T.; Farha, O. K. A facile synthesis of UiO-66, UiO-67 and their derivatives. *Chem. Commun.* **2013**, *49*, 9449-9451.
- (2) Lammert, M.; Wharmby, M. T.; Smolders, S.; Bueken, B.; Lieb, A.; Lomachenko, K. A.; Vos, D. D.; Stock, N. Cerium-based metal organic frameworks with UiO-66 architecture: synthesis, properties and redox catalytic activity. *Chem. Commun.* **2015**, *51*, 12578-12581.
- (3) Lammert, M.; Glissmann, C.; Reinsch, H.; Stock, N. Synthesis and Characterization of New Ce(IV)-MOFs Exhibiting Various Framework Topologies. *Cryst. Growth Des.* **2017**, *17*, 1125-1131.
- (4) Gedrich, K.; Senkovska, I.; Klein, N.; Stoeck, U.; Henschel, A.; Lohe, M. R.; Baburin, I. A.; Mueller, U.; Kaskel, S. A highly porous metal-organic framework with open nickel sites. *Angew. Chem. Int. Ed.* **2010**, *49*, 8489-8492.
- (5) Kim, I. S.; Borycz, J.; Platero-Prats, A. E.; Tussupbayev, S.; Wang, T. C.; Farha, O. K.; Hupp, J. T.; Gagliardi, L.; Chapman, K. W.; Cramer, C. J.; Martinson, A. B. F. Targeted Single-Site MOF Node Modification: Trivalent Metal Loading via Atomic Layer Deposition. *Chem. Mater.* **2015**, *27*, 4772-4778.
- (6) Toby, B. H.; Von Dreele, R. B., Gsas-II: The genesis of a modern open-source all purpose crystallography software package. *J. Appl. Crystallogr.* **2013**, *46*, 544-549.
- (7) Hammersley, A. P.; Svensson, S. O.; Hanfland, M.; Fitch, A. N.; Hausermann, D., Two-dimensional detector software: From real detector to idealised image or two-theta scan. *High Pressure Res.* **1996**, *14*, 235-248.
- (8) Juhás, P.; Davis, T.; Farrow, C. L.; Billinge, S. J. L., PDFgetX3: A rapid and highly automatable program for processing powder diffraction data into total scattering pair distribution functions. *J. Appl. Crystallogr.* **2013**, *46*, 560-566.
- (9) Wojdyr, M., Fityk: A general-purpose peak fitting program. *J. Appl. Crystallogr.* **2010**, *43*, 1126-1128.
- (10) Farrow, C. L.; Juhas, P.; Liu, J. W.; Bryndin, D.; Bozin, E. S.; Bloch, J.; Proffen, T.; Billinge, S. J., PDFfit2 and PDFgui: Computer programs for studying nanostructure in crystals. *J. Phys.: Condens. Matter* **2007**, *19*, 335219.
- (11) Schlenker, J. L.; Peterson, B. K. Computed X-ray powder diffraction patterns for ultrasmall zeolite crystals. *J. Appl. Crystallogr.* **1996**, *29*, 178-185.
- (12) Howarth, A. J.; Peters, A. W.; Vermeulen, N. A.; Wang, T. C.; Hupp, J. T.; Farha, O. K. Best practices for the synthesis, activation, and characterization of metal-organic frameworks. *Chem. Mater.* **2017**, *29*, 26-39.